ROBUSTNESS ASSESSMENT IN THE OPTIMIZATION OF LOW-PRESSURE DIE CASTING SUBJECT TO VARIATIONS IN SECONDARY ALLOY COMPOSITION

Alberto Vergnano, Hamed Rezvanpour, Marvin Spessotto and Francesco Leali
Universita degli Studi di Modena e Reggio Emilia Dipartimento di Ingegneria Enzo Ferrari, Modena, Italy

https://doi.org/10.1007/s40962-024-01504-4

Abstract

Porosity is a significant factor affecting the final mechanical properties in aluminum casting. Therefore, minimizing porosity by optimizing the casting parameters is of great importance. However, during normal production, some variability must be considered for these parameters, especially when using secondary alloys. Variations in alloy composition can greatly influence the solidification process, microstructure, and the product's mechanical properties. Accordingly, achieving a robust design that accounts for secondary alloy composition variations is crucial to ensure the consistent quality and performance of the cast parts. This research uses a car wheel as a case study for a low-pressure die casting process. An optimization process is then conducted using a genetic algorithm (GA) to refine casting parameters such as heat transfer coefficient (HTC) and initial pouring temperature. Finally, the results are analyzed using the signal-to-noise ratio and the Taguchi quality loss function method to measure the robustness of the design sets. These results indicated that by conducting an optimization process and introducing noise factors as parameters, a robust design that withstand alloy variations can be achieved, and a design of simulation experiment can be established.

Keywords: *aluminum casting, secondary alloys, low-pressure die casting, optimization, porosity, mechanical properties, Taguchi method, genetic algorithm, design of simulation experiments*

Introduction

There are two resources of Al alloys in the modern industry: primary Al, which is extracted from the Al-reach ores, (i.e. bauxite and laterite), and secondary Al alloys produced from recycled scraps. Primary production of Al has a substantial environmental impact, causing almost 2% of the global human-caused emissions in 2020 (1 billion metric tons of CO_2 equivalents). In addition to long-term environmental issues caused by primary production residues (red mud), the largest impact is generated by the high energy consumption of alumina reduction. Meanwhile, secondary Al alloys are produced through a far more energy-efficient method by recycling items at the end of their life cycle. Research has shown that the recycling process consumes 95% less energy than primary Al, making it a more environmentally friendly method.[1,2] Besides, using less amount of energy means cutting down production expenses; however, it is not without its disadvantages. In fact, the impurities and contaminants, such as Fe, which are present in the secondary alloy after multiple recycling or remelting processes, could potentially reduce mechanical properties, such as ultimate tensile, yield, and fatigue strengths, as well as decreasing its corrosion resistance. Therefore, more research should investigate the effects of utilizing secondary Al alloys in the industry. The Recycling Technologies for Circular Aluminum (RecAL) project,[3] funded by the European Union aims to facilitate paradigm shifts along the aluminum processing value chain. One of the most significant applications of secondary Al alloys is in the casting industry. A considerable amount of research is dedicated to enhancing the recycling and refining of Al alloys to make them suitable for casting processes, especially existing die-casting methods such as low-pressure die casting (LPDC).[4–7] When using secondary Al alloys, an important work package in RecAL is the robust design of the casting processes against different noise factors such as small variations in the alloy compositions.

Received: 18 September 2024 / Accepted: 20 November 2024
Published online: 27 December 2024

A robust process consistently makes high-quality products, even when there are changes in the manufacturing conditions and parameters. A methodology called robust design is employed to optimize such processes aiming to achieve specific objective performance.[8] Robust design uses a statistical methodology to design the experiments known as design of experiments (DOE). In DOE methodology, design parameters are set up with different levels, known as control factors. The uncontrollable factors in the process that might affect the final performance of the experiment are known as noise factors. The outcome, called the response, is statistically evaluated to define the optimized combination of design parameters that optimizes the process and also reduces performance variation around target values.[9]

DOE method has limited applications in the optimization of a LPDC process, since the mold involves a high investment and must be put into operational condition as soon as possible. Therefore, optimizing the mold and the process parameters through simulations is a perfect solution. Ye et al.[10] used the Taguchi method to refine the process variables for producing ZL205A cylindrical shell alloy parts through LPDC, and the results showed notable reduction in the porosity values of the castings. Zhang et al.[11] developed an artificial neural network (ANN) model that integrates a quantitative learning vector and backpropagation algorithm (BP) to map the LPDC process parameters and the intricate relationships among evaluation metrics. Also, they introduced a strategy that merges ANN with GA (genetic algorithm) to optimize the LPDC process. Gupta et al.[12] aimed to reduce casting defects in a silicon-based aluminum alloy carburetor housing. To this end, the GA optimization, combined with Fuzzy logic methodology (FLM) and the Taguchi method, was applied. These authors reported that solidifying-time and fill-up-time are the most sensitive parameters. Zhang et al.[13] conducted a multi-objective optimization of the AZ91D LPDC automotive wheel to minimize the shrinkage porosity and the secondary dendrite arm spacing based on software integration platform for engineering and scientific computation (SiPESC). To obtain better shrinkage porosity on an LPDC Al automotive wheel, Dhisale et al.[14] optimized the cooling channel parameters such as delay and duration of the cooling flow using multi-disciplinary design optimization (MDO) with a multi-physics simulation method. Accordingly, after optimization, they achieved a minimum total of 1.2% of shrinkage porosity. Zheng et al.[15] investigated the effect of latent heat in the solidification stage of an Al wheel produced by the LPDC method. These researchers simulated the solidification stage with different methods and compared the results with experimental models. As a result, they proposed the "Temperature Compensation Heat Capacity" as a new numerical approach to model the latent heat in solidification stage to obtain better results. Shahane et al.[16] implemented the Genetic Algorithm to the multi-objective optimization of Al LPDC. To this end, they used non-dominant sorting genetic algorithm (NSGA-II) to optimize the casting parameters, followed by training an algorithm based on neural networks to reduce the time and the cost for further simulations. Numerous studies have concentrated on the effect of various alloying compositions on aluminum alloy's final porosity and mechanical properties when using different casting methods.[17–23] However, these methods lack the capability to implement noise factors into the parameter optimization, making it difficult to study each parameter effect on the final solution. Therefore, methods such as sensitivity analysis should be considered to incorporate the effects of the noise factor into the GA. Despite extensive research on optimizing Al LPDC processes, few studies have explored using secondary aluminum alloys as casting materials while integrating GAs and robust design methods (e.g. Taguchi) to improve process parameter optimization.

Design of simulation experiment (DOSE) uses the observed findings from DOE to create accurate models for simulations. Based on the understanding and data gathered from the initial physical experiments (DOE), simulations are then designed and used to further explore and optimize the process. This method allows for more extensive experimentation and optimization without the cost and time associated with physical experiments. In the present work, DOSE techniques are implemented to improve the assessment of designs in the optimization task. The optimization is done using the GA method, and then, the composition variation in the secondary Al alloy is introduced as a noise factor, using the orthogonal array method. The goal is to seek an optimal set of design parameters for delivering the optimization objectives, while reducing the effects of variations in the secondary alloy.

The remainder of this paper is organized as follows. Section "Materials and Methods" discusses the materials, and the methods used in this study. Then, Sect. "Case Study on Optimizing an LPDC Process for an Aluminum Car Wheel" presents the report of a case study about a simulation of a LPDC Al wheel. Section "Results and Discussion" reports and discusses the results. Finally, Sect. "Conclusions" outlines the concluding remarks.

Materials and Methods

This section describes the method used in the paper to optimize the design parameters and improve the robustness, following the workflow shown in Figure 1. The method begins with creating a CAD model based on the requirements, followed by defining the initial process parameters, using both experimental data and data from previous simulations. The objective performances of the design must be defined, together with their tolerances. Next, the control factors must be defined for their range of

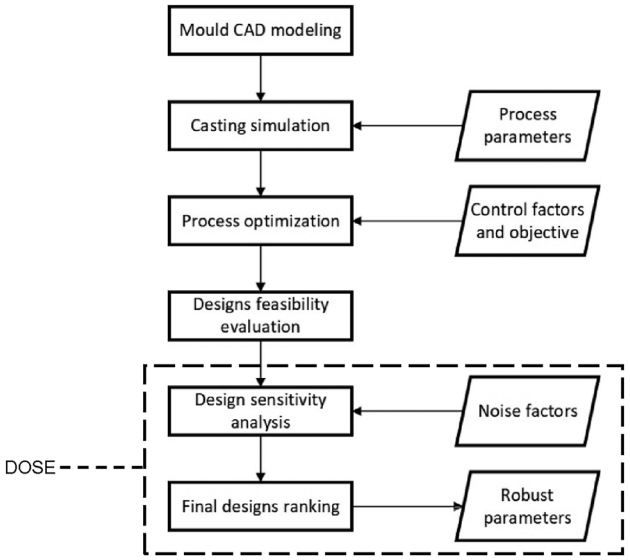

Figure 1. Optimization and DOSE workflow employed in this research.

variation and their possible levels. Design optimization is carried out through well-established techniques using GA. Only designs within tolerances for the performance objective are then passed to the next DOSE phase, where noise factors, such as variations in the AI alloy composition, are considered with an orthogonal array. A robustness index is computed for each nominally good design. Finally, the evaluation is performed by considering the design performances and their robustness.

Design Optimization using Genetic Algorithms

This research uses commercial casting simulation software, Magmasoft, to conduct the simulations and optimize the casting process. The models simulate the complete phases of the casting process, including mold preparation, thermoregulation, alloy pouring and cavities filling, solidification, casting extraction, and any post-treatment. The simulation also considers the warm-up and stabilizing processes, including some heating cycles before the production that is evaluated for results assessment.

The simulation software includes an optimization module, capable of optimizing all the design variables, including parametric geometries and casting process parameters, using the genetic algorithm (GA) optimization method. Establishing an optimization process contains 3 important steps: (1) choosing the design parameters and their respective levels (2) defining the range of levels and (3) defining one or more objectives. The important step after selecting the design parameters is to choose the initial population or the first set of genotypes as parents. Incorporating all the design parameters and their levels creates an extensive search domain. This domain should be simplified to efficiently explore and identify the initial parameters without evaluating every possible combination. In this research, the Sobol sampling method was adopted as recommended by the software optimization module. The optimization will subsequently be conducted over a chosen number of generations.

The GA optimization method runs as follows:

1. Initialize first generation using Sobol Sequence sampling method.
2. Evaluate the result of the simulations and fitness of the first generation.
3. Select the next generation parents based on their performance, considering the objective.
4. Perform the crossover and random mutation.
5. Replace the current generation with the next generation.
6. Continue the steps until a convergence occurs based on the objective.
7. Select and rank the best designs based on their performances.

Conducting GA optimization ensures that the process parameters are optimized and the objectives are achieved. However, since alloying composition variations cannot be incorporated directly as noise factors in the analysis, an additional step is necessary. This involves implementing these variations as controllable factors, similar to process parameters, by using the DOSE method.

Design of Simulation Experiments

This subsection includes simulating the effects of variations in alloy composition as noise factors on the performance of the final casting. A simulation model cannot consider noise factors, so the composition of the secondary alloys is changed as an input parameter in the process.

The alloying composition percentages are considered as the input parameters for the second phase of the simulation sequences use the orthogonal array to cover the variety of alloying composition changes. Orthogonal arrays provide a systematic way to organize experiments efficiently, and they are denoted by the notation $L_{experiments}\left(levels^{factors}\right)$. For instance, the orthogonal array $L_9\left(3^3\right)$ describes 9 experiments for 3 factors with 3 levels each. This notation ensures that the experimental setup covers a comprehensive range of conditions for the factors being tested. To create an orthogonal array, one begins by conducting a preliminary analysis of the variations in the secondary alloys. This analysis helps determine the appropriate number of levels and factors that need to be included in the experiments. Based on this, an orthogonal array can be defined to suit the specific needs of the study. The array is then combined with the previous optimization phase, resulting in a complete experimental plan. The resulting

orthogonal array gives equal importance to all parameter levels, ensuring that each is weighted the same. In this way, the time and the cost required for experimental trials are significantly reduced.

Robustness Assessment for Final Design Ranking

To assess the robustness of the design during the optimization phase, the robustness indexes are defined as follows.

The first index is the signal-to-noise ratio (S/N), calculated over the repeated experiments. A higher, lower or nominal S/N ratio indicates that the design performance is better relative to the noise, indicating a more robust design. When the optimization has a nominal-is-better objective the S/N is computed as:[24]

$$SN_n = -10\log\left[(Y_0 - \mu)^2 + \sigma^2\right] \quad \text{Eqn. 1}$$

where Y_0 is the specific objective and σ^2 is the process variance.

When the optimization has a higher-is-better objective, the S/N becomes:[24]

$$SN_l = -10\log\left[\frac{1}{n}\sum\nolimits_{i=1}^{n}\frac{1}{\{(y\}_i)^2}\right] \quad \text{Eqn. 2}$$

with $Y_0 =$, while with a lower-is-better optimization the S/N is expressed as:[25]

$$SN_s = -10\log\left[\frac{1}{n}\sum\nolimits_{i=1}^{n}\{(y\}_i)^2\right] \quad \text{Eqn. 3}$$

with $Y_0 = 0$.

Another potential index is the quality loss (QL) defined by Taguchi as:[26,27]

$$\mathrm{QL} = \mathrm{L}(Y) = \mathrm{K}[Y - Y_0]^2 = (\mu - Y_0)^2 + \sigma^2 \quad \text{Eqn. 4}$$

QL represents a decrease in signal quality caused by the noise or other unexpected factors. The greater the QL, the lower the quality of the objective and therefore the quality of the process. QL is more useful than S/N as it also provides information about the process mean, the variance, and the target.

Case Study on Optimizing an LPDC Process for an Aluminum Car Wheel

This section presents a case study on optimizing a mold to produce a car wheel with LPDC.

Simulation of the LPDC for an Aluminum Car Wheel

All the CAD models are designed and assembled in SolidWorks and then imported in casting simulation software, as shown in Figure 2a. The mold consists of a base with a bottom insert, sliding side inserts, and an upper side insert. The material used for the mold and the inserts is H11 or 1.2343 steel. The other details, including the inlet, runner, and a gate, are added to the casting system as the CAD model is symmetric—only half of the model is used in the simulations, saving substantial time. The casting is done using secondary AlSi7Mg0.3, with its composition and physical properties outlined in Table 1. To effectively manage the temperature field, the design includes cooling channels and resistor heaters. These components will be crucial in the optimization phase, influencing the design parameters. All the components were meshed using software's meshing tool. Mesh sizes are determined based on each component's role in critical casting stage. For instance, a mesh size of 2.5 mm was applied to the casting metal and the inner parts of cavities in direct contact with it, 5 mm was applied for the cooling channels and gate and runner, and 50 mm was applied for the mold parts.[28] Figure 2b illustrates the mesh sizing and quality.

To begin the simulation, initial conditions for the surrounding environment and the molten material are considered as reported in Table 2. The whole LPDC process is modeled as follows: a preparation phase of 60 s, a pouring and solidification phase of 450 s, a casting extraction for 30 s, and finally the casting is air-cooled until it reaches 100 °C. The casting process follows the pressure curve shown in Figure 3 with an initial pouring phase pressure, the filling pressure, and the holding stage pressure. These pressures are considerably higher than those of previous stages to help feeding any possible shrinkages in the solidification phase. Note that the pressure curve is applied at the inlet in the simulation model, and it must be increased in a LPDC machine to consider the distance from the crucible below.

The model is completed by defining the heat transfer coefficient (HTC) between any pair of contacting CAD parts. The most important HTC is between the alloy and the mold, which must consider the insulating coating on the surfaces and the solidification shrinkage. A typical insulating coating of a medium thickness, suggested by the software, is used in the model. From database property and from experience, the HTC between the Al and the mold is defined in two stages: 1) it is set to 620 W/m^{2}K at temperatures above the liquidus, and 2) 400 W/m^{2}K at temperature below the solidus. To evaluate steady production conditions, 9 heating cycles were simulated prior to the final production cycle. This number of preparatory cycles is essential, as the mold requires proper heating before beginning the actual production cycle. Three

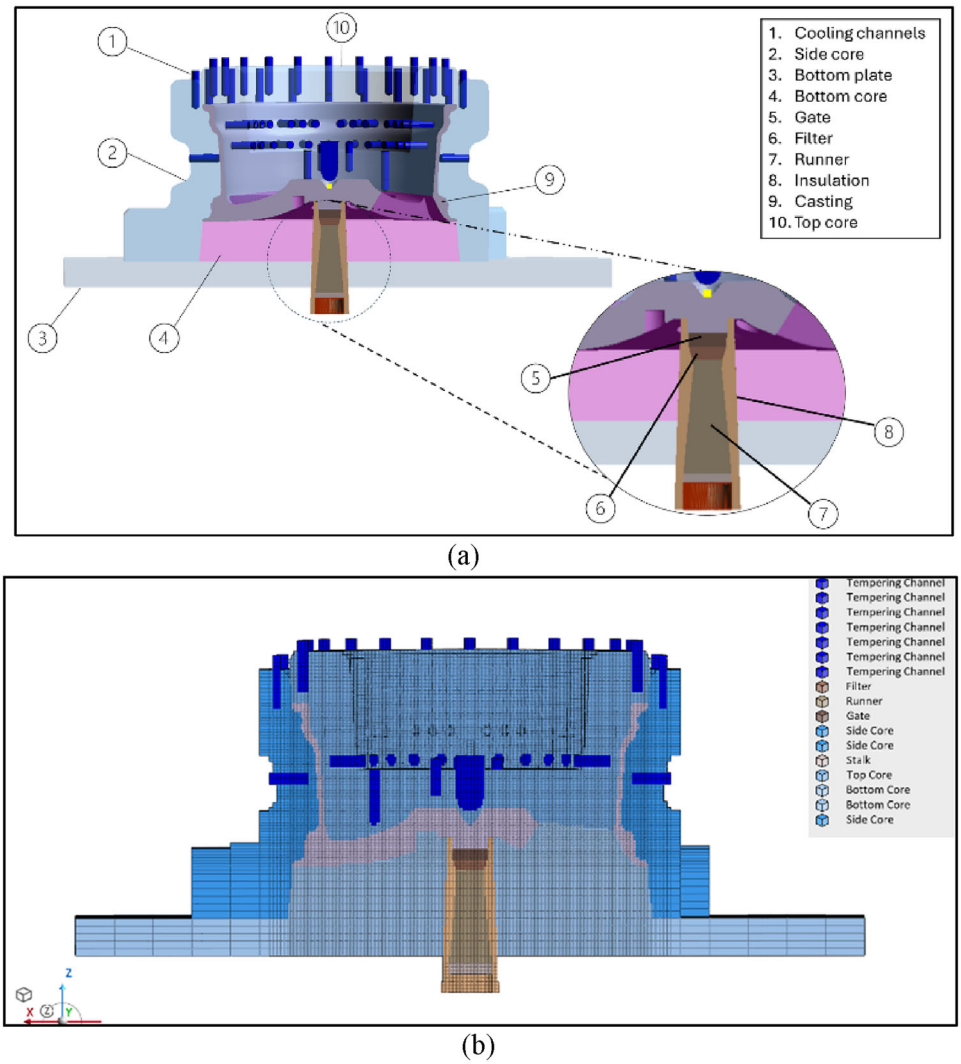

Figure 2. (a) CAD and (b) mesh models.

thermocouples were positioned at various locations within the mold to accurately monitor the temperature gradient throughout the heating cycles as illustrated in Figure 4. This approach effectively simulates a preheated mold with a non-uniform temperature field. Initial temperatures for the first cycle were set at a constant 200 °C for all inserts and 100 °C for the base. Figure 5 shows the mold temperature gradient before and after the heating cycles. According to Figure 6, after 9 cycles, the mold temperature stabilizes, reaching a steady-state optimal for initiating the production cycle. The metal pouring temperature is set to 720 °C. The heating energy from the crucible beneath the mold is also considered into the simulation. It is necessary to guarantee filling with speeds lower than 0.5m/s at every point of the mold to avoid any air entrapments. Note that all the cavity cells are filled with temperatures higher than the liquidus temperature of the alloy.

The filling stage was completed in 12 s, followed by exposing the part to the solidification stage with holding pressure for 450 s. Figure 7 present the temperature progress of the casting material during the filling stage. As can be seen, the temperature is lower at the points where two separate metal flows converge, and this pattern remains the same throughout the filling process. Figure 8 depicts the liquid percentage in the solidifying alloy in different time intervals.

The analysis of the solidification with the fraction liquid method shows that in some areas the percentage of solidified material deviates from the expected sequential solidification. Figure 9 illustrates a critical observation at the location where porosities are detected. The liquid metal content is measured at 79.3% in this area, with values of 87.7% above and 85.6% below just before the separation. Considering the feeding effectivity set at 30.0%, the sequent result reveals the separation, with liquid percentages of 59.2, 71.2 and 67.2% in the same picked points. These measurements indicate that the liquid metal percentage does not follow the expected pattern of decreasing along the solidification direction. Consequently, a region remains in the feeding effectivity phase while the

Table 1. Al Alloying Compositions

Alloying element	Percentage
CR	0.00
CU	0.03
FE	0.50
H	0.00
MG	0.40
MN	0.30
NA	0.00
NI	0.10
P	0.00
SB	0.00
SI	7.00
SR	0.00
TI	0.15
ZN	0.10

Table 2. Initial Casting Parameters

Parameter	Quantity
Solidus temperature	542 °C
Liquidus temperature	613 °C
Niyama criterion temperature	549 °C
Thermo criteria temperature	615 °C
Initial pouring temperature	720 °C
Latent heat	430.5180 KJ/Kg
Feeding effectivity	30%
Surface tension coefficient	0.8 N/M
Rheology model	Newtonian

surrounding material undergoes solidification, and it is not capable to flow anymore. The lack of sufficient material feed and inadequate pressure to compensate for the shrinkage during solidification, results in the formation of significant shrinkage porosity. This phenomenon is mainly because of the thickness difference between the areas. Since minimizing the porosity is the primary goal of the design, this observed results are clearly unacceptable, thus, the casting parameters must be optimized in the simulation model. The optimization method employed in this study is the GA, which is integrated in software's optimization module. The mold cooling is critical in the LPDC process, as it mainly influences the solidification progress, and consequently impacts some factors such as microstructure and porosity.

During the solidification stage, the heat is removed from the molten metal through the cavity walls by circulating coolant flow, usually water, inside the cooling channels. The sequential solidification which results in a quality casting is led by the amount of heat exchanged during this phase. Therefore, the HTCs at the surfaces of the cooling channels are managed as design parameters to be optimized. To obtain the HTC related to the cooling channels, it is necessary to adjust the cooling flow rate inside the channels. The HTC is estimated by software from the following parameters:

- Diameter of the cooling channels [mm].
- Cooling duct length [mm].
- Flow rate [m3/h].
- Cooling fluid temperature (i.e. 50 °C in this study).

The alloy pouring temperature is another optimization parameter since it modifies the temperature field of the mold. All of the design parameters in the optimization are reported in Table 3. As mentioned before, the primary goal of the optimization is to minimize the porosity to below 5% in total. It should be noted that a small probability of porosity is unavoidable in die casting and must be estimated based on experience. The porosity results are displayed only for values with an occurrence probability above 5% and within a 5–10% range. According to foundry calibration, a probability of less than 5% indicates a negligible occurrence, 5–10% indicates a progressive increase from occasional to frequent, and more than 10% signifies an inevitable occurrence.[29] In Figure 10, a detailed cross-sectional view is presented, highlighting the internal structure of the mold and its component. All the component names also addressed in Table 3.

The initial search space in GA refers to the total number of unique genotypes possible, considering various levels of each parameter. It represents all possible combinations of parameter values that the algorithm can explore. The parameter ranges for HTC in different cooling channels are defined by analyzing previous simulations, temperature gradients and solidification patterns. In this paper, there are 6 design parameters in the optimization process, with 5 levels each. Therefore, the total search space is $5^6 = 15625$. The initial genotypes are selected with Sobol. Convergence is influenced by the parameters of the design variables specified in the initial sequence, since the algorithm must first explore the design space and recognize trends. For this reason, the initial population should be selected in a way that covers the entire search space, without wasting computation power. As a general guideline, following equation is used for determining the number of initial designs:

$$N_{IP} = N_{obj} \times N_{dv} \times 2 \begin{cases} \text{If } N < 16 & N_{IP} = 16 \\ \text{If } N > 16 & N_{IP} = N \end{cases} \quad \text{Eqn. 5}$$

where N_{IP} stands for the number of initial populations, N_{obj} is the number of objectives, and N_{dv} is the number of

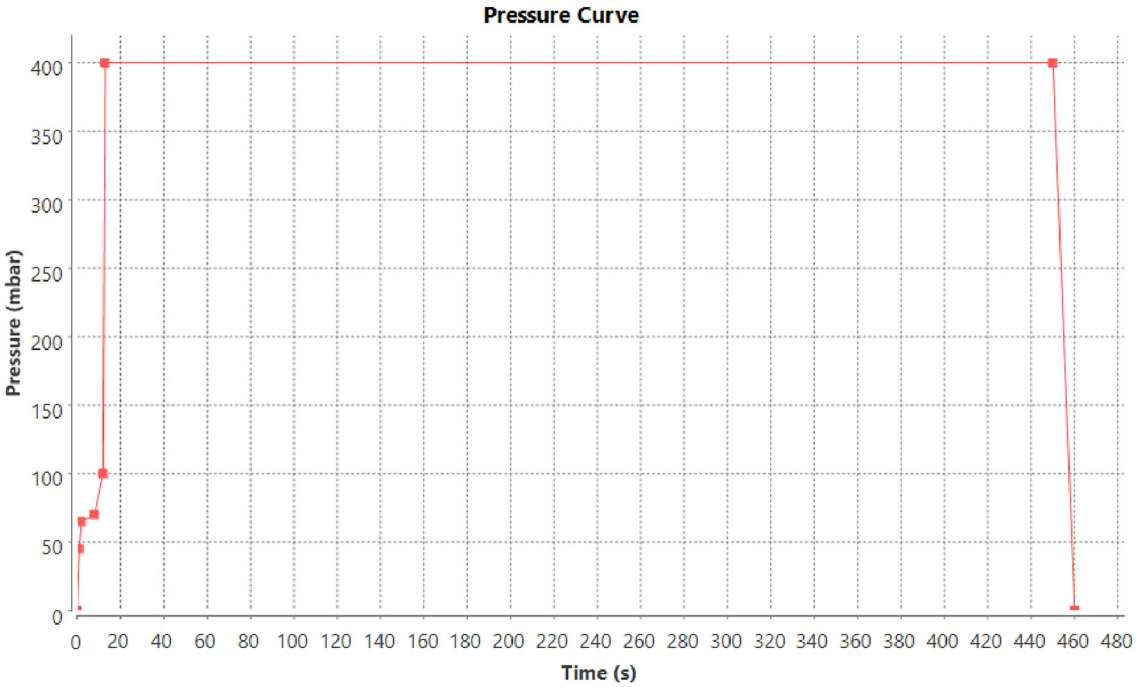

Figure 3. Pressure curve for alloy pouring in the simulation of LPDC.

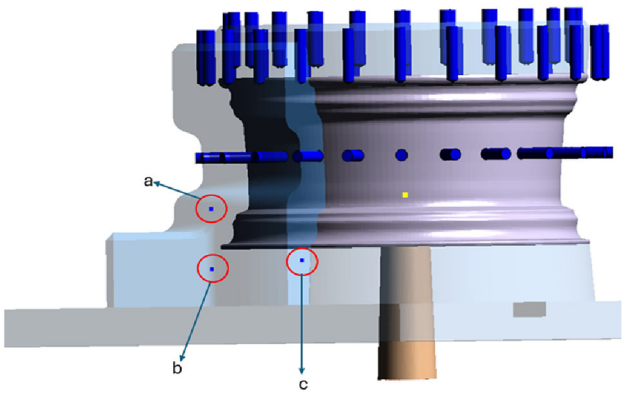

Figure 4. Thermocouples in different locations: (a) TC_02_Side_upper, (b) TC_01_Side_lower, (c) TC_03_lower_insert.

design variables. In this this case, because the product is equal to 10, which is smaller than 16, the number of the designs in the initial population is considered as 16. The optimization runs for 10 generations. As a closed-source software, the optimization module determines the mutation probability and the crossover function. Figure 11 represent the liquid percentage in the solidifying alloy in different time intervals after GA optimization is completed. Following the optimization, sequential solidification occurs precisely as intended, and no further separation is observed.

Figure 12 depicts the historical chart of optimization parameters with their optimal convergence attained after the simulation generation. These parameters converged and lead to zero porosity throughout the wheel, although the porosity in the hub would be accepted as the wheel is subsequently machined. Table 4 reports the parameters for the first 10 designs in the ranking of the optimization assessment and the results of the optimization in terms of porosity.

The analysis of the porosity percentage in all 10 designs shows that the optimization meets the objective, reducing the overall porosity to under 5%. To identify the most robust design against alloying composition variations among these 10 optimized design sets, the DOSE method and S/N analysis were applied, incorporating composition variations as noise factors using the orthogonal array described in the previous sections.

Design of Simulation Experiments on LPDC for a Car Wheel

In the DOSE phase, the noise factors are implemented into the casting simulations. Slight variations in 4 alloying elements are considered as noise factors. Silicon (Si) is the most important component in Al alloys. This element improves the mechanical properties of the alloy, the viscosity and the shrinkage porosities. Iron (Fe) is the most undesirable impurity in secondary alloy. This metal has low solubility within Al and significantly decreases the corrosion resistance of the final alloy. The formation of Al–Fe intermetallic elements improves the tensile strength of the alloy, despite lowering its ductility. Zinc (Zn) has good solubility within AI, and it is used to increase the alloy's strength, hardness and workability, but it lowers corrosion

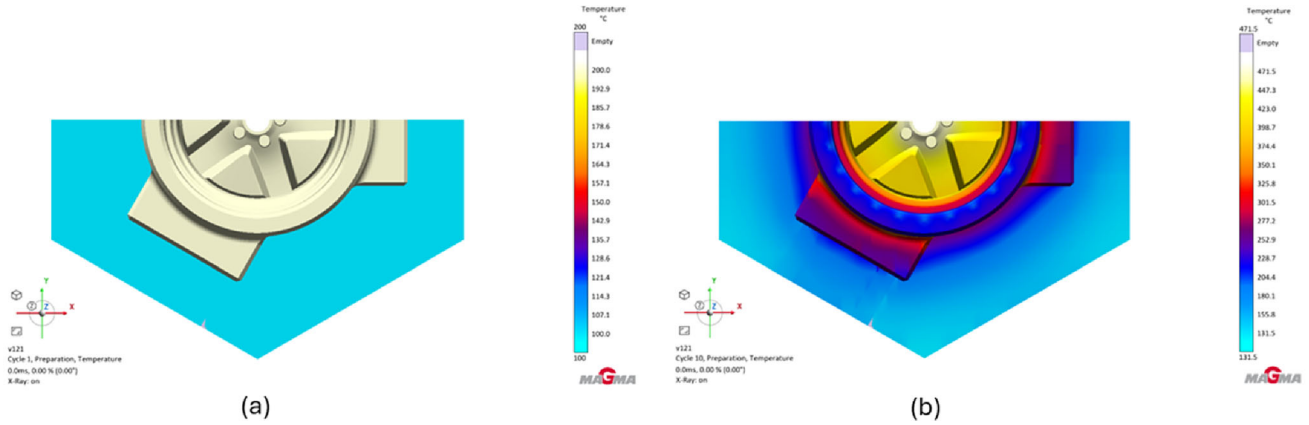

Figure 5. (a) Mold temperature gradient before heating cycles, (b) after 9 heating cycle.

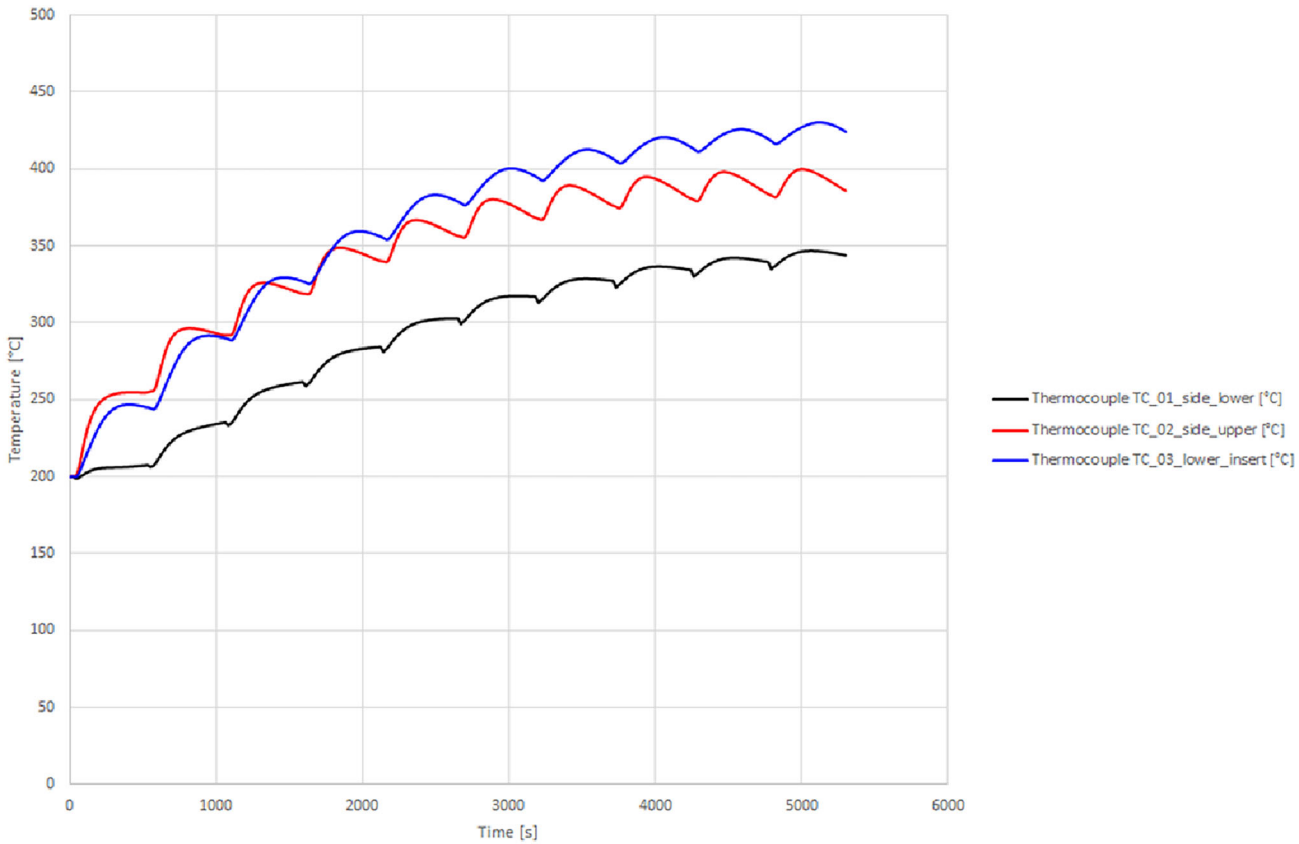

Figure 6. Temperature profile over time for different thermocouple positions in different heating cycles.

resistance. Chromium (Cr) is used as a corrective buffer against the unwanted iron. It increases the yield and tensile strength without decreasing ductility. Therefore, there are 4 varying parameters, each with 3 levels as shown in Table 5.

The impact of the noise factors on the outcome was analyzed using an L_9 orthogonal array to vary these factors systematically. This method allows identifying key trends and design efficiency. Table 6 presents the orthogonal array used for implementing the noise factors into the casting as process parameters. The top 10 designs from the GA optimization were recalculated 9 times, to analyze the effect of the alloy composition variation on the final porosity percentage.

The porosity results are reported in Table 7, expressed in total mm^3 volume, where the first column is the nominal AlSi7Mg0.3 as from the $L_9(3^4)$ array.

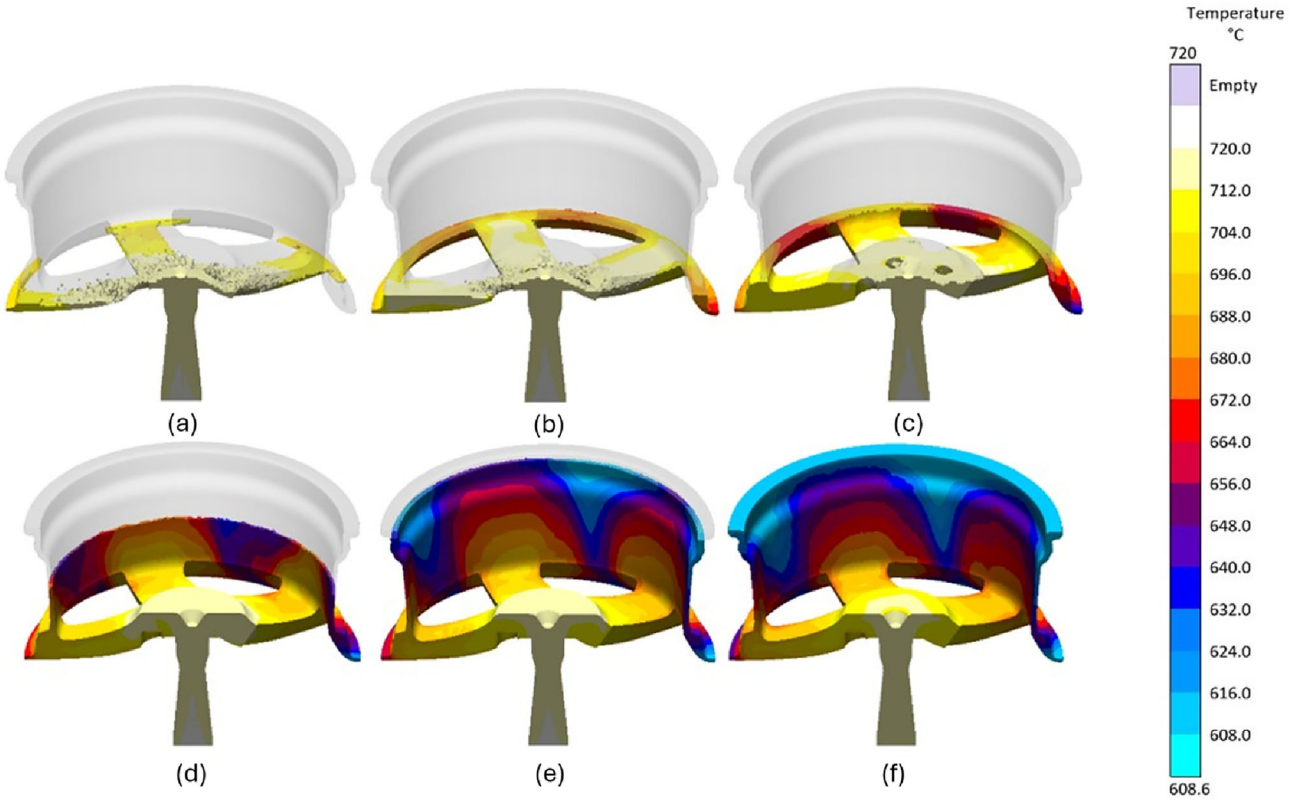

Figure 7. Temperature gradient in filling stage: (a) 2.2 s; (b) 4.4 s; (c) 6.6 s; (d) 8.8 s; (f) 11 s.

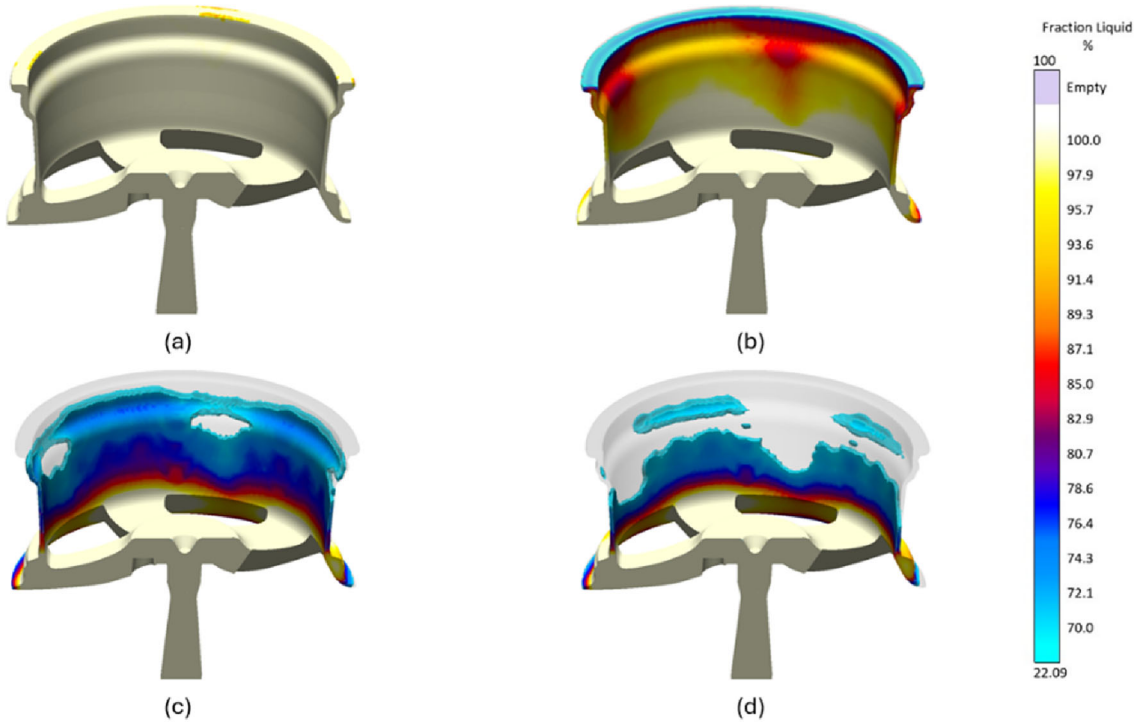

Figure 8. Fraction liquid: (a) after 12 s; (b) after 16 s; (c) after 22 s; (d) after 24 s.

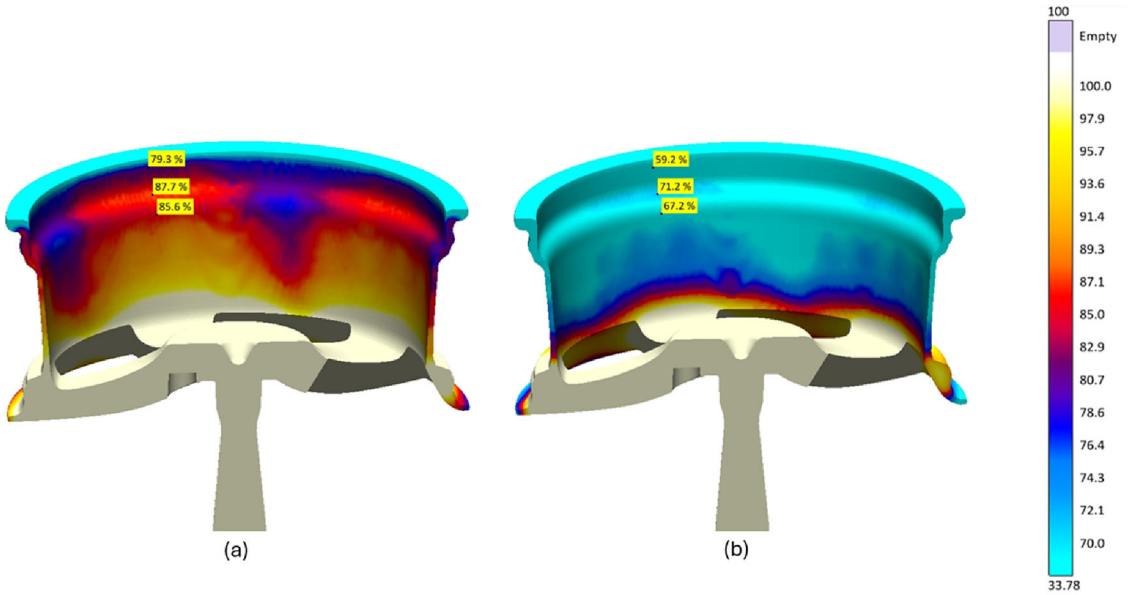

Figure 9. Hot spot of liquid material above feeding effectivity percentage (a) before the separation; (b) after the separation.

Table 3. Optimization Parameters and Levels

Parameters	Levels
Cooling channel up	500, 1000, 1500, 2000, 2500 W/m^{2}K
Cooling channel surface Ext	100, 300, 500, 700, 900 W/m^{2}K
Cooling channel surface Int	0, 100, 200, 300, 400 W/m^{2}K
Cooling channel down	500, 1000, 1500, 2000, 2500 W/m^{2}K
Cooling channel down Int	2200, 2400, 2600, 2800, 3000 W/m^{2}K
Pouring temperature	700, 710, 720, 730, 740 °C

Results and Discussion

After simulating the casting with variations in the alloying compositions and collecting all the data, S/N ratio analysis and QL function were used to evaluate the robustness of each design. Table 8 reports the signal-to-noise ratio index for each selected design considering the porosity. According to the table, Design 2 has mostly very low porosity values (almost all 1×10^{-9}), except for one outlier at 8.9. This outlier, while large, does not significantly affect the overall average, leading to a relatively better S/N ratio compared to designs with multiple large porosity values. Therefore, the overall quality is better with less variation around the target, which is desirable in the "smaller is better" S/N approach. In the "smaller is better" criterion, when using the logarithmic S/N ratio, the goal is to have the S/N value closer to zero, which means less negative values are better. All designs are finally reranked based on their S/N ratio index.

Figure 13 reports the significance of every control factor on the final porosity based on the S/N ratio analysis for each factor as follows:

For each controlling factor, the non-null (non-NaN) values are extracted. Then, the mean of the squared values is computed:

$$\text{mean squared} = \frac{1}{n}\sum_{i=1}^{n} x_i^2 \qquad \text{Eqn. 6}$$

where x_i are the individual values and n is the number of values. Then, the S/N is computed using Formula (3). After calculating S/N, all the numbers are normalized through a scale between 0 and 1, and a heatmap is crated based on this normalization. The analysis showed that the HTC Surf Int is the most significant parameter with a normalized factor of 1. It is in a good correlation with the geometry of the mold, as the HTC_Surf_int is the HTC parameter for the closest cooling channel to where the first porosity happened. In other words, it has the biggest impact on the final porosity of the casting. The initial temperature and the HTC Surf Ext are ranked next with factors of 0.58 and 0.5, respectively.

Using Taguchi quality loss function is another method to analyze the data to choose the best design. The Taguchi QL function measures the deviation of the observed values from a target value Y_0 and helps in identifying the design that minimizes this deviation. Based on Eq. (4) and

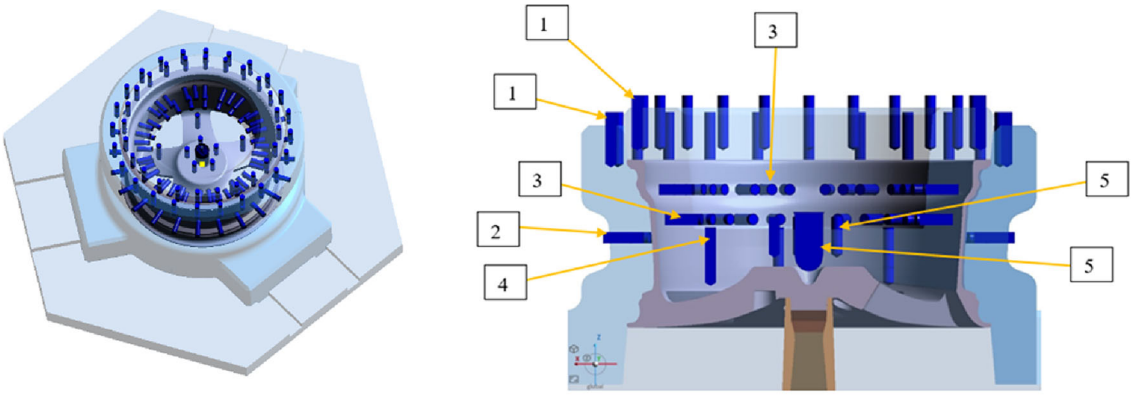

Figure 10. Complete model for the optimization with 5 circular sets of cooling.

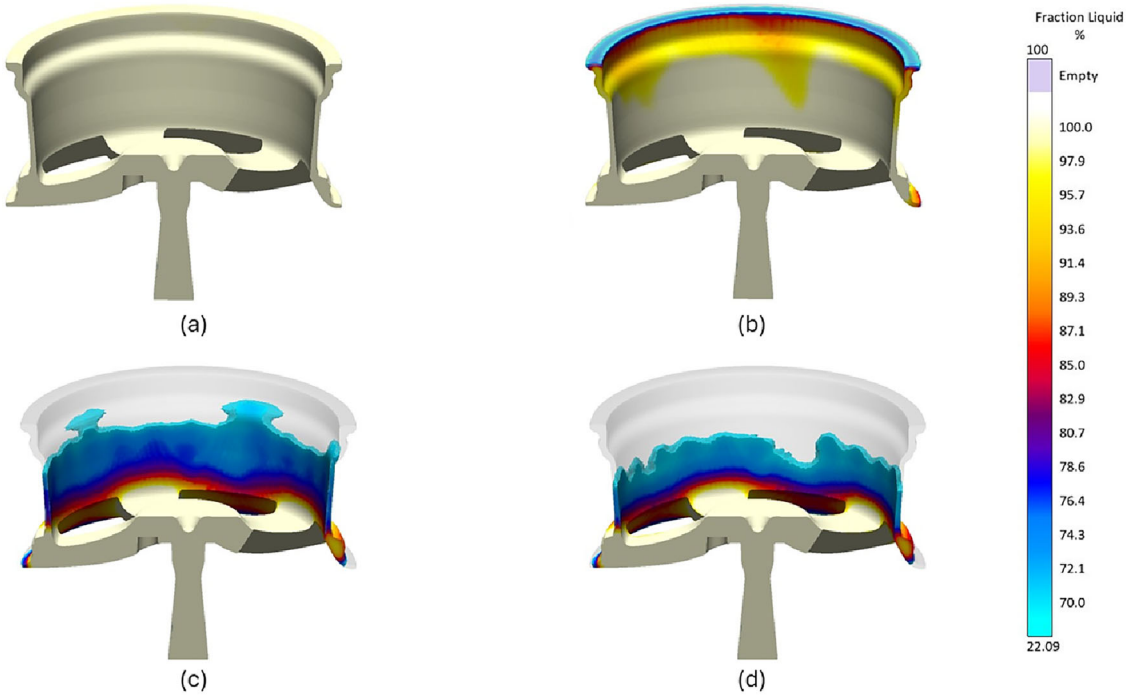

Figure 11. Porosities result for the optimized LPDC simulation of the wheel casting in 2nd generation in fraction liquid: (a) after 12 s; (b) after 16 s; (c) after 22 s; (d) after 24 s.

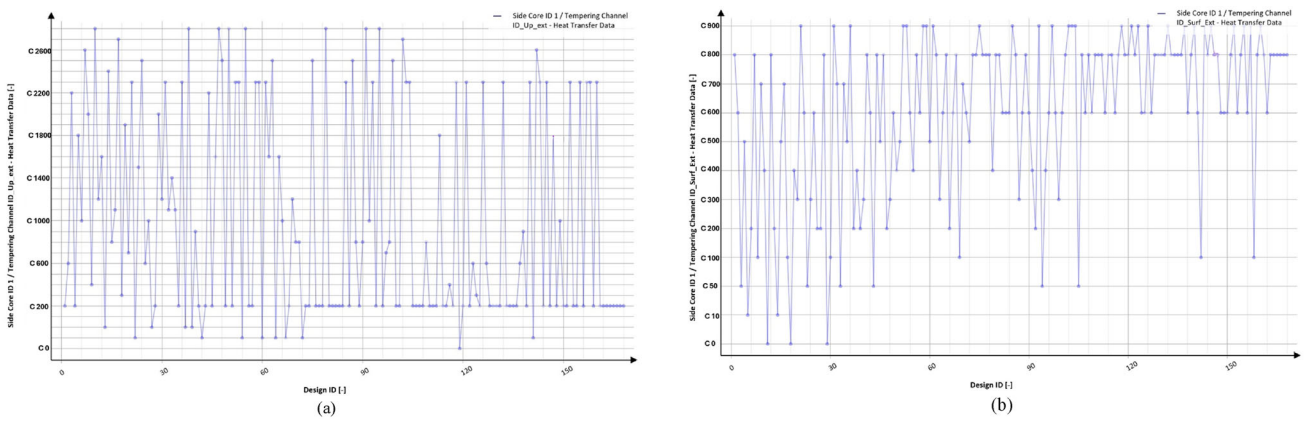

Figure 12. The historical chart of optimization parameters for (a) Cooling channel up; (b) Cooling channel surface Ext.

Table 4. Optimized Design Parameters

Rank	Design	Up_ext	Surf_ext	Down_ intern	Down	Up	Surf_int	Down_ Center	Up_in	Surf_ up_in	Initial Temp.	Porosity
1	147	1800	900	3000	1500	1900	300	2500	2800	300	720	0.000463
2	160	2300	1000	3000	2100	1900	300	2300	2800	200	730	0.000474
3	149	1000	700	3000	1500	1900	300	2500	2800	200	720	0.000657
4	152	200	700	3000	1400	2000	200	2500	1000	200	720	0.000679
5	146	200	900	3000	1500	2200	200	2500	2800	200	720	0.000737
6	107	200	700	3000	1500	1900	300	2500	2800	200	720	0.000875
7	104	2300	1000	2600	2100	2000	300	1800	1000	100	730	0.00101
8	121	2300	1000	2600	2100	2400	300	1800	1000	100	730	0.00141
9	122	200	900	3000	1500	2000	200	2500	1000	200	720	0.0027
10	158	200	900	3000	1500	2400	200	2500	1000	200	700	0.00344

assuming the $Y_0 = 0$ (target porosity), design 2 stands out with the lowest quality loss. Therefore, it is the most effective in minimizing deviation from the target porosity, making it the best choice for robustness against alloying composition variations. All the data calculated with Ql function is presented in Table 9 and Figure 14.

In Figure 14, the first plot shows the mean porosity for each of the 10 designs. Design 10 has the highest mean porosity, indicating it deviates significantly from the desired target of zero. Design 2, on the other hand, exhibits one of the lowest mean porosities, further supporting its suitability based on the QL function analysis. The other designs exhibit varying levels of mean porosity, with design 4 also showing a relatively low mean porosity but not as low as design 2. The second plot, which displays the standard deviations of porosity for each design, provides insight into the consistency of each design. A lower standard deviation shows more consistent results. Design 2 again performs well, showing a moderate standard deviation. In another words, its porosity measurements are relatively consistent. In contrast, design 4 has the highest standard deviation, suggesting that its porosity results are highly variable and thus less reliable despite its low mean porosity. Lastly, the QL plot explicitly shows the calculated QL for each design, where lower values indicate better performance. The minimal quality loss of design 2 reaffirms its effectiveness in achieving the target porosity with minimal deviation. Design 10, with the highest QL, is the least desirable, indicating significant deviations from the target value. The visual representation of QL helps to quickly identify which designs are most robust and reliable.

Considering the orthogonal array for alloying composition variations, the signal-to-noise ratio analysis was done to measure the effect of each alloying material on the final porosity. Figure 15 and Table 10 report information about the S/N analysis for each alloying composition. The

Table 5. Alloy Composition Variation Levels

Parameters	Levels (%)
Si	7, 7.25, 7.5
Fe	0.5, 0.65, 0.8
Zn	0.1, 0.15, 0.2
Cr	0, 0.075, 0.15

Table 6. $L_9(3^4)$ *Orthogonal Array for the Composition of the Secondary Alloy*

Composition	Fe	Si	Cr	Zn
1	0.5	7	0	0.1
2	0.5	7.25	0.075	0.15
3	0.5	7.5	0.15	0.2
4	0.65	7	0.075	0.2
5	0.65	7.25	0.15	0.1
6	0.65	7.5	0	0.15
7	0.8	7	0.15	0.15
8	0.8	7.25	0	0.2
9	0.8	7.5	0.075	0.1

analysis shows that Cr has the most significant effects on the porosity with a S/N ratio that demonstrates a steep negative slope, indicating that increasing Cr levels result in a considerable decrease in porosity. The effect of Fe, Sr, and Zn on the final porosity is also notable, but less compared to Cr. The main effect plot for Fe shows a significant drop at the 0.65 level, followed by a slight increase,

Table 7. Porosity Results for the $L_9(3^4)$ DOSE Considering Composition Variations

Design	Composition								
	1	2	3	4	5	6	7	8	9
1	1e-9	1e-9	1e-9	1e-9	1e-9	1e-9	1e-9	1e-9	12.519
2	1e-9	1e-9	1e-9	8.9	1e-9	1e-9	1e-9	1e-9	1e-9
3	1e-9	1e-9	1.8	2.4	1e-9	10.78	1e-9	1e-9	1e-9
4	1e-9	1e-9	4.66	3.6	30.85	5.61	5.8	1e-9	1e-9
5	1e-9	2.4	1e-9	4.8	4.32	6.8	1e-9	2.034	1e-9
6	1e-9	1e-9	1.023	6.7	7.89	1e-9	1e-9	2.086	1e-9
7	1e-9	5.22	5.1	8.9	1e-9	1e-9	1e-9	1e-9	5.085
8	1e-9	6.56	1e-9	11.52	1e-9	1e-9	1e-9	1e-9	1e-9
9	1.07	5.8	1e-9	3.4	1.08	1e-9	3.1	6.073	1.172
10	1.09	2.2	9	21.1	9.3	4.1	25.6	5.2	1e-9

Table 8. S/N Index for the Porosity Objective

Rank	Design	Porosity S/N
1	Design 2	−9.44538
2	Design 9	−10.252
3	Design 5	−10.3627
4	Design 6	−10.9706
5	Design 1	−12.409
6	Design 7	−12.4531
7	Design 8	−12.9064
8	Design 3	−14.2344
9	Design 4	−20.6757
10	Design 10	−21.6565

Table 9. QL Index for the Porosity Objective

Design	Mean	Standard deviation	Variance	Quality loss
Design 1	1.391	3.934	15.479	17.414
Design 2	0.989	2.797	7.823	8.801
Design 3	2.664	4.406	19.413	26.512
Design 4	5.613	9.273	85.325	116.834
Design 5	2.262	2.399	5.756	10.871
Design 6	1.967	2.939	8.637	12.504
Design 7	2.701	3.209	10.299	17.592
Design 8	2.009	3.936	15.491	19.527
Design 9	2.411	2.188	4.787	10.597
Design 10	8.621	8.492	72.114	146.438

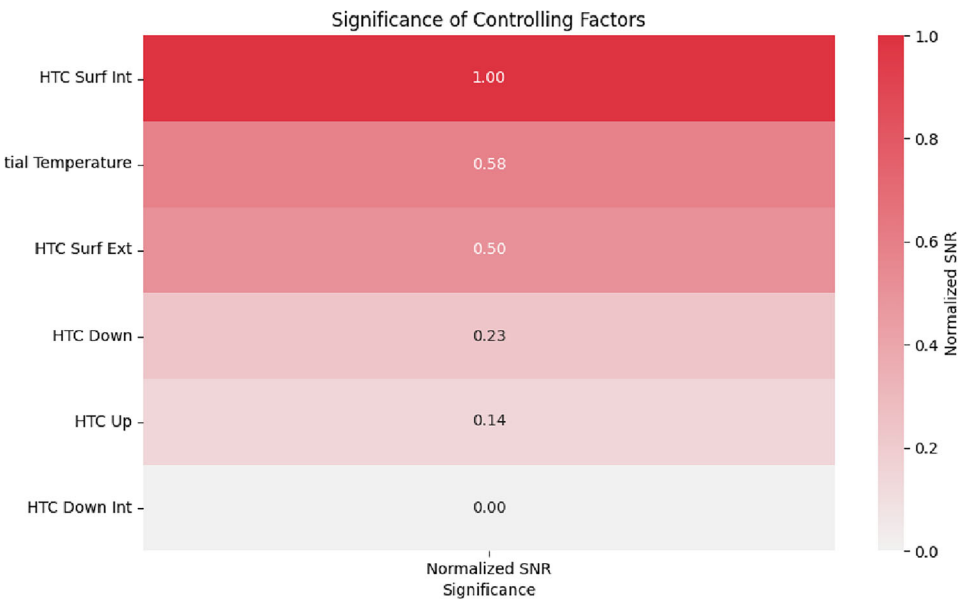

Figure 13. Control factor contribution on the S/N.

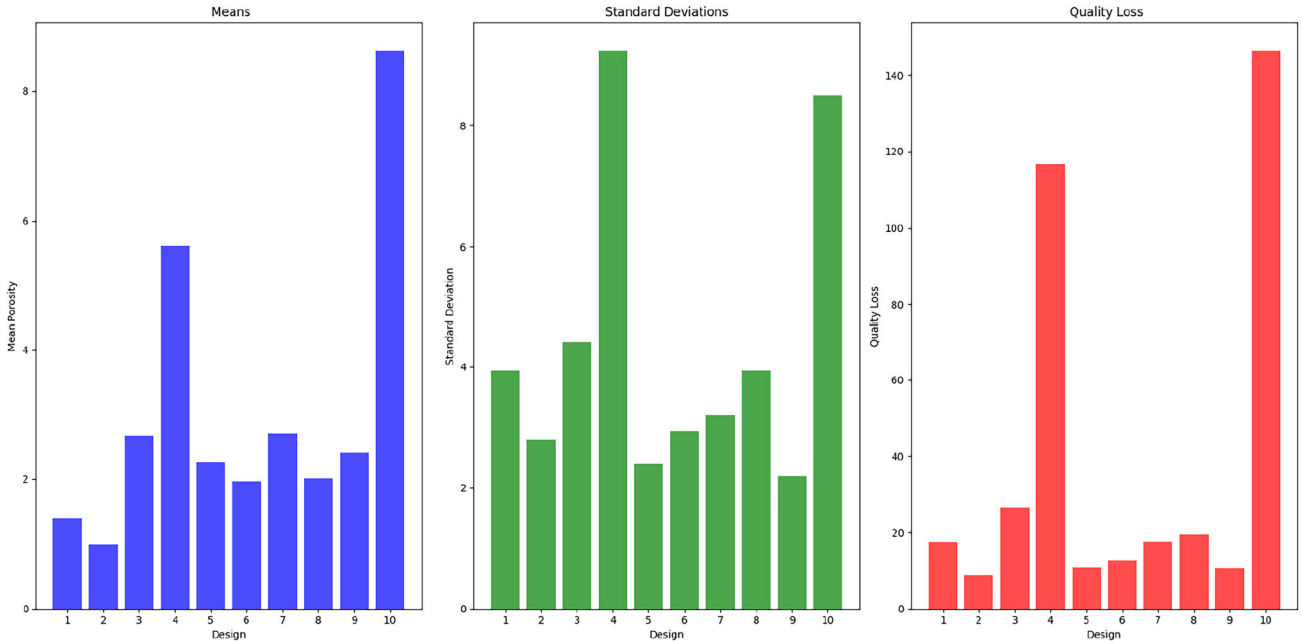

Figure 14. Linear graph in QL function, (a) mean values; (b) standard deviation; (c) QL function.

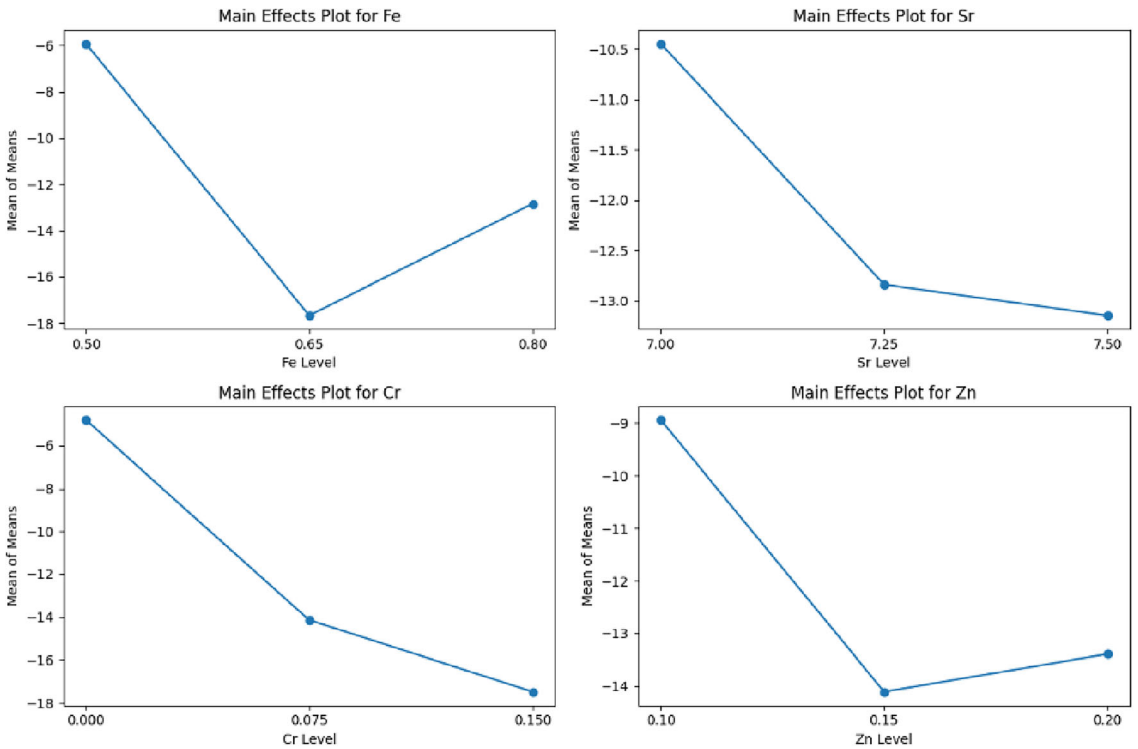

Figure 15. S/N ratio analysis for alloying compositions.

indicating an optimal level for minimizing porosity. For Sr value, the plot suggests a consistent decrease with increasing percentage. Hence, the minimum level would be the optimal one.

Conclusions

This paper studies the effect of alloy composition variation on the final product porosity level in a low-pressure die casting (LPDC) automotive wheel using design of

Table 10. The S/N Ratio and Rankings

Material Levels	Fe	Sr	Cr	Zn
1	−5.929	−10.445	−4.798	−8.94
2	−17.662	−12.84	−14.15	−14.103
3	−12.843	−13.148	−17.485	−13.391
Delta	11.733	2.702	12.686	5.163
Rank	2	4	1	3

simulation experiment (DOSE) and genetic algorithm (GA) optimization methods. A CAD model of the automotive wheel was developed using CAD software. The model was then imported into Magmasoft casting simulation software for pre-processing and initial parameter definition. After setting the initial parameters, casting simulations were conducted to evaluate these parameters and their impact on the final product's porosity. After analyzing the porosity levels in the final product and identifying the porosity locations, the genetic algorithm (GA) method was applied to optimize the heat transfer coefficient (HTC) levels in the cooling channels and the initial pouring temperature, aiming to achieve a global porosity level below 5%. After running the optimization for 10 generations, all parameters showed good convergence, and the resulting parameter sets were ranked based on their achieved porosity levels.

To evaluate the robustness of the optimized designs against variations in alloy composition, the top 10 design sets were selected for the DOSE phase. Subsequently, an L9 orthogonal array was applied to incorporate composition variations into these selected designs, focusing on four key alloying elements in secondary alloys: Fe, Cr, Si, and Zn. Each of the 10 chosen designs was simulated 9 times with different composition sets defined by the orthogonal array. The results were then analyzed using the signal-to-noise (S/N) ratio and Taguchi quality loss (QL) function. All 10 designs are ranked again based on their S/Nand QL score. The analysis revealed that design 2 is the most robust against the alloy composition variation as it performed better in both S/N and QL analysis. Two additional S/N ratio analyses were conducted to examine the influence of each process parameter and alloying element on porosity. As shown in Figure 10, the HTC parameter in cooling channel No. 3 (HTC_Surf_Int) has the greatest effect on controlling porosity, correlating well with the mold geometry, as this channel is closest to the porosity-prone area on the wheel flange. The second S/N analysis evaluated the significance of each alloying element on porosity; according to Table 10, Chromium (Cr) has the most substantial impact on reducing porosity, followed by Iron (Fe). This result is consistent with practical applications, where Cr is often used to counteract the negative effects of Fe and aid in grain refinement.

In this paper, a novel approach was introduced to incorporate noise factors, such as alloy composition variations, into the genetic algorithm (GA) optimization process using design of simulation experiments (DOSE) methods. By implementing this approach, the study demonstrates that noise factors, like alloy composition variations, can effectively be integrated as process parameters within the DOSE framework. This enables a detailed assessment of each parameter's impact on the final objective function, leading to more robust and reliable designs that maintain performance even under varying conditions. This method proves valuable for advancing casting processes that rely on secondary alloys, where compositional variations are common. Although this paper addresses the theoretical aspects of the problem, future work could involve experimental studies to validate the reliability of the DOSE methodology and simulation results. Additionally, a more detailed investigation into porosity and SDAS under real-world conditions would enhance understanding and confirm the robustness of these optimized designs in practical applications.

Funding

This study was supported by HORIZON EUROPE Framework Programme, 101138747, Alberto Vergnano.

Open Access

REFERENCES

1. H. Nunes, O. Emadinia, R. Soares, M.F. Vieira, A. Reis, Adding value to secondary aluminum casting alloys: a review on trends and achievements. Mater. (2023). https://doi.org/10.3390/ma16030895
2. S.K. Padamata, A. Yasinskiy, P. Polyakov, A review of secondary aluminum production and its byproducts.

Jom **73**(9), 2603–2614 (2021). https://doi.org/10.1007/s11837-021-04802-y
3. E. Union, The Recycling Technologies for Circular Aluminium (RecAL) project.
4. A. Vergnano, U. Bergamini, D. Bianchi, P. Veronesi, R. Spagnolo, F. Leali, Simulation and experimental validation of secondary dendrite arm spacing for AlSi7Mg0.3 chassis parts in low pressure die casting. In: Advances on Mechanics, Design Engineering and Manufacturing III: Proceedings of the International Joint Conference on Mechanics, Design Engineering & Advanced Manufacturing, Springer International Publishing. (2021)
5. E. Anglada, A. Meléndez, I. Vicario, E. Arratibel, G. Cangas, Simplified models for high pressure die casting simulation. Procedia Eng. **132**, 974–981 (2015). https://doi.org/10.1016/j.proeng.2015.12.585
6. H. Puga, J. Barbosa, T. Azevedo, S. Ribeiro, J.L. Alves, Low pressure sand casting of ultrasonically degassed AlSi7Mg0.3 alloy: modelling and experimental validation of mould filling. Mater. Des. **94**, 384–391 (2016). https://doi.org/10.1016/j.matdes.2016.01.059
7. D. Závodská, E. Tillová, I. Švecová, L. Kuchariková, M. Chalupová, Secondary cast Al-alloys with higher content of iron. Mater. Today Proc. **5**, 26680–26686 (2018). https://doi.org/10.1016/j.matpr.2018.08.135
8. G.-J. Park, T.-H. Lee, K.H. Lee, K.-H. Hwang, Robust design: an overview. AIAA J. **44**, 181–191 (2006). https://doi.org/10.2514/1.13639
9. M. Arvidsson, I. Gremyr, Principles of robust design methodology. Qual. Reliab. Eng. Int. **24**, 23–35 (2007). https://doi.org/10.1002/qre.864
10. W. Ye, W. Shiping, N. Lianjie, X. Xiang, Z. Jianbing, X. Wenfeng, Optimization of low-pressure die casting process parameters for reduction of shrinkage porosity in ZL205A alloy casting using Taguchi method. Proc. Ins. Mech. Eng. Part B: J. Eng. Manuf. **228**, 1508–1514 (2014). https://doi.org/10.1177/0954405414521065
11. L. Zhang, L. Li, S. Wang, B. Zhu, Optimization of LPDC process parameters using the combination of artificial neural network and genetic algorithm method. J. Mater. Eng. Perform. **21**, 492–499 (2011). https://doi.org/10.1007/s11665-011-9933-0
12. K. Gupta, S. Kumar, P. Chandna, G. Bhushan, Optimization of process parameters during pressure die casting of a380: a silicon-based aluminium alloy using GA & fuzzy methodology. SILICON **13**(8), 2429–2443 (2020). https://doi.org/10.1007/s12633-020-00594-z
13. C. Zhang, Y. Fu, H. Wang, H. Hao, Multi-objective optimization of process parameters during low-pressure die casting of AZ91D magnesium alloy wheel castings. China Foundry **15**, 327–332 (2018). https://doi.org/10.1007/s41230-018-8066-6
14. M. Dhisale, J. Vasavada, A. Tewari, An approach to optimize cooling channel parameters of low pressure die casting process for reducing shrinkage porosity in aluminium alloy wheels. Mater. Today Proc. **62**, 3189–3196 (2022). https://doi.org/10.1016/j.matpr.2022.03.478
15. Q. Zheng, Y. Xiao, T. Zhang, P. Zhu, W. Ma, J. Liu, Numerical simulation of latent heat of solidification for low pressure casting of aluminum alloy wheels. Metals (2020). https://doi.org/10.3390/met10081024
16. S. Shahane, N. Aluru, P. Ferreira, S.G. Kapoor, S.P. Vanka, Optimization of solidification in die casting using numerical simulations and machine learning. J. Manuf. Process. **51**, 130–141 (2020). https://doi.org/10.1016/j.jmapro.2020.01.016
17. B. Callegari, T.N. Lima, R.S. Coelho, the influence of alloying elements on the microstructure and properties of Al–Si-based casting alloys: a review. Metals (2023). https://doi.org/10.3390/met13071174
18. Y. Ma, Y. Liu, M. Wang, Microstructures and corrosion resistances of hypoeutectic $Al_{-6.5}Si_{-0.45}$ Mg casting alloy with addition of Sc and Zr. Mater. Chem. Phys. (2022). https://doi.org/10.1016/j.matchemphys.2021.125321
19. E.A. Elsharkawi, M.F. Ibrahim, A.M. Samuel, H.W. Doty, F.H. Samuel, Understanding the effect of be addition on the microstructure and tensile properties of Al–Si–Mg cast alloys. Int. J. Metalcast. **16**, 1777–1795 (2021). https://doi.org/10.1007/s40962-021-00715-3
20. J. Kasinska, D. Bolibruchova, M. Matejka, The influence of remelting on the properties of $AlSi_9Cu_3$ alloy with higher iron content. Materials (2020). https://doi.org/10.3390/ma13030575
21. M. Kaba, A. Donmez, A. Cukur, A.F. Kurban, H.E. Cubuklusu, Y. Birol, $AlSi_5Mg_{0.3}$ alloy for the manufacture of automotive wheels. Int. J. Metalcast. **12**, 614–624 (2017). https://doi.org/10.1007/s40962-017-0191-2
22. G. Timelli, D. Caliari, J. Rakhmonov, Influence of process parameters and Sr addition on the microstructure and casting defects of LPDC A356 alloy for engine blocks. J. Mater. Sci. Technol. **32**, 515–523 (2016). https://doi.org/10.1016/j.jmst.2016.03.010
23. Y. Wang, H. Liao, Y. Wu, J. Yang, Effect of Si content on microstructure and mechanical properties of Al–Si–Mg alloys. Mater. Des. **53**, 634–638 (2014). https://doi.org/10.1016/j.matdes.2013.07.067
24. J.-L. Wen, Y.-K. Yang, M.-C. Jeng, Optimization of die casting conditions for wear properties of alloy AZ91D components using the Taguchi method and design of experiments analysis. Int. J. Adv. Manuf. Technol. **41**, 430–439 (2008). https://doi.org/10.1007/s00170-008-1499-0
25. D.H. Wu, M.S. Chang, Use of Taguchi method to develop a robust design for the magnesium alloy die casting process. Mater. Sci. Eng. A **379**, 366–371 (2004). https://doi.org/10.1016/j.msea.2004.03.006

26. S. Maghsoodloo, The exact relation of Taguchi's signal-to-noise ratio to his quality loss function. J. Qual. Technol. **22**, 57–67 (2018). https://doi.org/10.1080/00224065.1990.11979206
27. E.A.C. Naresh, K. Sharma, K.M. Ragsdell, K. Paryani, Quality loss function—a common methodology for three cases. J. Ind. Syst. Eng. **1**, 218–234 (2007)
28. P.G.B. Oliveira de Santos, L.F. Gomes, J.E. Spinelli, Solidification and strength behavior of A356 Al alloy wheels. Int. J. Metalcasting (2024). https://doi.org/10.1007/s40962-024-01286-9
29. A. Vergnano, E. Salvati, A. Magistrelli, E. Brambilla, P. Veronesi, F. Leali, A method for yield and cycle time improvements in Al alloy casting with enhanced conductivity steel for die construction. Manuf. Rev. (2022). https://doi.org/10.1051/mfreview/2022017